Describing Seasonal Differences in Tree Crown Delineation Using Multispectral UAS Data and Structure from Motion

Nicholas E. Kolarik[a]*, G. Ellis[b], A. E. Gaughan[a] and F. R. Stevens[a]

a. Department of Geography and Geosciences, University of Louisville, Louisville, KY, USA 40292
b. Department of Anthropology, University of Louisville, Louisville, KY, USA 40292

*Corresponding author; nicholaskolarik@gmail.com

This is an Accepted Manuscript of an article published by Taylor & Francis Group in *Remote Sensing Letter* on 03/06/2019, available online https://www.tandfonline.com//10.1080/2150704X.2019.1629708

Describing Seasonal Differences in Tree Crown Delineation Using Multispectral UAS Data and Structure from Motion

Abstract

Unmanned Aerial Systems (UAS) have emerged as a platform capable of providing valuable data on vegetation structure, health, and productivity. The platform provides maximum temporal flexibility in data collection and customizability of spatial footprints which is important for mapping and monitoring vegetation conditions especially for high spectrally and structurally heterogeneous landscapes. In this letter, we investigate the potential improvement in structural information when using sensor payloads that include infrared bands (730-810 nm) in addition to the typical visible bands of many UAS sensor payloads. Specifically, we use derived point clouds and imagery collected from UAS-mounted sensors at a test site in Louisville, Kentucky, USA to assess whether multispectral sensors improve estimates of vegetation structure for plant greenness (leaf-on) and senescence (leaf-off) periods. Results indicate that including detailed multispectral reflectance information beyond the visible portion of the electromagnetic spectrum aids in estimating structural characteristics of woody vegetation, regardless of season. While both leaf-on and leaf-off periods result in reasonable crown height estimates, leaf-on conditions also improve radial estimates, likely due to continuous canopy surfaces. These findings advance research for remote sensing analyses assessing structural composition in heterogeneous landscapes where varying levels of vegetation structure have implications on land use and land function.

1. Introduction

Remotely-sensed structural information on the environment has transformed scientific understanding of landscape conditions and phenomena. Early methods specific for collecting data on ecosystem structure were time consuming and labor intensive (Avery and Burkhartn 2001). However, unmanned aerial systems (UAS) provide flexibility for collection of fine-resolution imagery at low-cost (Zahawi et al. 2015). UAS are effective for quantifying vegetation structure and estimating fractional vegetation coverage (Cunliffe, Brazier and Anderson 2016; Mayr et al. 2017). Low altitude flights produce centimetric ground sampling distances much finer than data collected via satellite platforms. Despite these advantages, understanding how extending the spectral range of sensor payloads past the typical RGB range and combination with finer spatial grain and temporal fidelity of UAS data to increase of structural information in vegetation characteristics is less documented.

Reflectance in the near-infrared (NIR) portion of the electromagnetic spectrum is useful for analyses of vegetation health and coverage extent (Tucker 1979; Curran 1980). Reflected energy in the wavelengths between 700 nm and 900 nm can be leveraged to detect photosynthetically active vegetation, as plant cells with healthy active chlorophyll are excellent reflectors of energy in this portion of the spectrum (Tucker 1979). In addition, while NIR reflectance is widely used with other bands for various ratio-based proxies for greenness and vegetation health (e.g., Normalised Difference Vegetation Index (NDVI)), the red edge (680 - 750 nm) has been found to be one of the best descriptors of active chlorophyll content in remote sensing (Filella and Penuelas 1994). It is this transition from the red to the NIR where reflectance is particularly sensitive to phenological changes in productivity and the same characteristics that make it useful for distinguishing within-flight vegetation characteristics complicate between flight standardization and comparison. That said, spectral information in the red edge and NIR are seasonally variable and have potential for informing the extraction of structural information in a heterogeneous landscape.

In the lab, advances in computer vision and photogrammetric techniques enable researchers to translate high resolution image datasets into three-dimensional surface information otherwise unattainable from these data (Dandois and Ellis 2010). Approaches such as Structure from Motion with Multi-View Stereo (SfM-MVS) have proven capable of creating three-dimensional point clouds comparable to those acquired through higher cost laser scanning techniques such as LiDAR (airborne and terrestrial laser scanners) (Salami, Barrado, and Pastor 2014). With the

SfM-MVS approach, aerial photos with a high degree of overlap are used to identify features and key points to produce a sparse point cloud (SfM) which is then densified (MVS) producing a point cloud to be analyzed in the same manner as data collected by LiDAR, the current standard for three-dimensional data products (Smith, Carrivick, and Quincey 2016). From these densified point clouds, high resolution two-dimensional products such as orthomosaics, digital surface models (DSM), and digital terrain models (DTM) can be derived, offering datasets that can be analyzed similarly to traditional aerial or satellite imagery.

This letter addresses how to leverage the visible portion of the electromagnetic spectrum along with the transition (i.e. red edge, 730-740 nm) and near-infrared ranges (730-810 nm) of a modern, UAS-ready sensor for estimating height and radial dimensions of woody individuals. We analyze forest structure at E.P. "Tom" Sawyer Park, a mixed-use recreation area in Louisville, Kentucky, USA and compare tree crown delineations and classification of vegetation based on structural characteristics from two different time periods representing periods of greenness (leaf-on) and senescence (leaf-off). We investigate whether height and crown estimates using SfM-MVS point clouds derived from data collected beyond the visible spectrum into the near infrared (NIR more closely resemble *in situ* measurements within a region of interest.

2. Data and methods

2.1 Study area

The test site chosen was a plot located in E.P. "Tom" Sawyer state park, a mixed-use recreation area in Louisville, Kentucky offering opportunities for measurement of various vegetation structures, such as trees, shrubs, and grasses (Figure 1). An unkept portion of the park was chosen to more closely resemble less managed landscapes. Flights conducted during senesced conditions (November 2017) and leaf-on conditions (July 2018) provide opportunities for methodological comparisons of the influence of multispectral data collection beyond the visible portion of the spectrum and seasonality in a site dominated by deciduous vegetation.

2.2 UAS data

The platform utilized for this study was the DJI Mavic Pro, a micro quadcopter, outfitted with two sensors: a three-axis gimbal stabilized 12-megapixel RGB camera attached to the quadcopter itself (DJI, Shenzhen, China), and the Parrot Sequoia multispectral sensor mounted below the aircraft with a sunlight irradiance sensor mounted above. Well within the payload capacity of the platform, this sensor collects narrowband imagery in green (530-570 nm), red (630-670 nm), red-edge (730-740 nm), and near-infrared (NIR) (770-810 nm) portions of the electromagnetic spectrum (Micasense 2018).

One flight was conducted in early November with the goal of capturing images exhibiting high spectral heterogeneity due to varying levels of senescence across many species present in the plot, and a second flight conducted in late July captured full leaf-on conditions with closed, continuous canopy surfaces in many parts of the study area. The November flight was conducted in overcast conditions and the July flight in clear conditions. Both ideal for consistency among data collected via UAS survey, differences in light and reflectance are normalised through the use of the sunlight irradiance sensor included in the Parrot Sequoia rig described above (Pix4D 2017).

Pre-programmed flight plans and the autonomous capabilities of the DJI Mavic Pro were used for 200 x 200-m double-grid flight patterns at 100-m altitude and navigated using on-board GNSS and the Mavic's inertial measurement unit. Photos were captured to ensure 85% frontal overlap and 70% side overlap at minimum, sampling the study area according to recommendations for UAS image acquisition in the SfM-MVS workflow suggested in the user manual (Pix4D 2017). Flights were conducted at midday to minimize shadow effects and images obtained exhibited ground sampling distances of ~3.7 cm (Mavic RGB sensor) and ~10.4 cm (Parrot Sequoia).

2.3 UAS data processing

Images collected from both sensors were processed using Pix4Dmapper version 3.3 software package (Pix4D, Lausanne, Switzerland). Optimal processing parameter values were chosen through systematic testing of isolated settings to identify deviations from the software defaults that improved the quality of the output products. With the high resolution RGB point cloud as the baseline, point clouds generated for each band of Sequoia data were generated and compared against the point cloud for the Mavic RGB data with respect to agreement with *in situ* measurements. We assume that higher spatial resolution of RGB data in bands that overlap between sensors (green, red) will provide stronger estimates, but to identify the utility of the Sequoia data, particularly in the red edge and NIR bands, point clouds for each band were analyzed individually.

Geolocation of each point cloud was performed within the Pix4D SfM workflow by leveraging location information stored in the EXIF tag of each photo. Using the on-board navigation system of the Mavic as well as the internal GNSS within the Parrot Sequoia, point clouds were accurately placed in three-dimensional space without the use of ground control (Turner, Lucieer, and Wallace 2014). This method provides reasonable location accuracy (sub-meter) in a small fraction of the time required for an intensive ground control survey (Padró et al. 2019).

2.4 In-situ data collection methods

At the test site, a total of 34 woody individuals were opportunistically sampled based on access to a clear line of sight for both the stem and top of the crown. Stem locations were recorded at sub-meter accuracy using a Garmin R1 GNSS receiver (Garmin, Olathe, KS, USA) and heights were estimated by taking the mean of three height measurements taken using a Leica Disto 810 rangefinder (Leica Geosystems, Aarau, Switzerland). In the four cardinal directions, crown radial measurements were recorded for each woody individual. Due to inherent location error, resulting tree crown polygons were moved manually to align with the individuals measured in the imagery.

2.5 Delineation of woody individuals

Testing the influence of spectral information beyond that of the visible portion of the spectrum on delineation of woody individuals is addressed through analysis of each point cloud produced through the SfM-MVS process. Densified point clouds for the RGB Mavic imagery as well as each narrowband sensor of the Sequoia were analyzed using the ENVI LiDAR version 5.2 software package. Trees were estimated by providing the software simple threshold information for both height and radial metrics. This study defines tree heights between 3 and 50 m and radial measurements between 1 and 6 m. These thresholds were chosen to be representative of mature, non-shrub woody species, representative of many that may be present in field site locations across temperate- and savanna-based forest environments. Point clouds were used to derive a DSM and DTM from which a canopy height model (CHM) is estimated by subtracting the DTM from the DSM. Maxima that lie above set thresholds that do not exhibit shape and textural characteristics similar to buildings or power lines are classified as trees. Through this local estimation of tree canopies, heights and radial dimensions of each estimated tree produce an associated vector for proceeding analysis.

A selection query used to detect tree vectors that intersected *in situ* measurements served to reduce the total number of output vectors to those that overlapped *in situ* measurements. However, due to the highly condensed nature of the vegetation in the study area and possibility of detecting multiple height maxima within a single crown, overlapping tree vectors were common, thus requiring subsequent manual analysis to reduce these clusters individually and visually identify the single estimate produced that would best serve as representative for *in situ* measurements in these instances. This process allowed for *in situ* measurements to be directly compared to vector output from ENVI LiDAR.

Additionally, to analyze the accuracy of areas delineated as trees in the ENVI LiDAR processing, 100 random points were generated and field validated to determine the appropriate class (tree/non-tree) for each point. Points were differentially corrected to minimize GNSS error following collection, though still not reduced below decimetric accuracy levels. Comparison of

the tree vector estimates from the SfM MVS and ENVI LiDAR workflow and field validation is intended to provide an understanding of associated quantity error (*Q*) and allocation error (*A)* using a confusion matrix following Pontius and Millones (2011). These measures are meant to provide measures of disagreement between estimates and validation data in a straightforward manner, as Pontius and Millones (2011) show the kappa family of indices to be inadequate although pervasive statistics for describing agreement in land cover analysis.

3. Results

The November data collected exhibited a Mavic RGB point cloud with an average point cloud density of 66.85 points/m^2 while Sequoia data resulted an average point cloud density of 7.98 points/m^2 . Point densities varied substantially between seasons, however, with the Mavic RGB point cloud density increasing to 197.8 points/m^2 and Sequoia point clouds decreasing in density slightly to 5.55 points/m^2 in the July datasets.

The total number of *in situ* measured woody individuals estimated by these point clouds ranged from 25 to 32 of 34 measured depending on the spectral band and season. No one band or season combination successfully estimated all woody individuals but the RGB and red edge had the highest estimated sample at 32 in the senesced and leaf-on periods respectively. Visual assessment of the output also revealed that trees were overestimated at times. Based on the 100 random points identified as tree/non-tree, the allocation disagreement was minimized marginally by the red and green point clouds in November ($A = 0$) and the RGB in July ($A = 0.04$). Quantity disagreement was lowest among the RGB data in November ($Q = 0.14$) and green data in July ($Q = 0.101$).

Height estimates among point clouds produced from November data shown in Figure 2 revealed strongest agreement with field measurements as described by the coefficient of determination (R^2) and mean absolute error (MAE) using the red ($R^2 = 0.66$, MAE = 1.15, $n = 29$) and green point clouds ($R^2 = 0.66$, MAE = 1.354, $n = 26$), followed by the red-edge point cloud ($R^2 = 0.6$, MAE = 1.17, $n = 25$). The NIR point cloud shows less agreement than the other individual bands ($R^2 = 0.18$, MAE = 1.93, $n = 27$) but was still minimized error in UAS estimates compared to the RGB data ($R^2 = 0.27$, MAE = 6.11, $n = 32$). And while the RGB point cloud delineated the most tree crowns, it seems there was a systematic overprediction in height estimates as indicated in the RGB scatter (Figure 2).

The July data exhibit the strongest agreement with using point-rich RGB data ($R^2 = 0.74$, MAE = 1.941, n = 29) followed closely by the red edge data ($R^2 = 0.71$, MAE = 2.99, $n= 32$) and NIR data ($R^2 = 0.66$, MAE = 3.38, $n = 33$). Performing poorly by comparison were the red ($R^2 = 0.55$, MAE = 4.36, $n = 31$) and green bands ($R^2 = 0.47$, MAE = 3.72, $n = 31$). These results compared to the November data are consistent with what we would expect due to the sensitivity of red and NIR reflectance values to vegetation phenology and the presence of active chlorophyll (Tucker 1979; Curran 1980), as productivity is less variable in the study area in July.

Direct comparison of results from radial estimate tests are less straightforward (Figure 3). The most effective datasets for estimating crown dimensions in autumnal conditions was the red edge point cloud ($R^2 = 0.63$, MAE = 0.97, $n = 25$) and the red point cloud ($R^2 = 0.3$, MAE = 1.3, $n = 29$). However, the red edge and red datasets only identified 25 and 29 of 34 sampled woody individuals respectively, a smaller sample than 32 identified using RGB data. RGB data, while consistently overestimating radial dimensions, more closely resemble the field data ($R^2 = 0.07$, MAE = 1.46, $n = 32$) than green but not the NIR point cloud. Furthermore, each of the point clouds derived from Parrot Sequoia data severely under predict radial measurements in senesced conditions, as well as have plots exhibiting heteroscedastic scatter, with greater variation in estimates associated with larger *in situ* radial measurements.

4. Discussion

With such vast differences in point cloud densities and concomitant spatial resolutions, it would be reasonable to expect inferior results from the Sequoia sensor based on its shortcomings in spatial detail alone, but the coarser, multispectral data show better ability to describe structural characteristics, particularly when productivity is variable among species present.

Providing full canopy surfaces seem to result in stronger delineation efforts due to minimal within object heterogeneity compared to leaf-off conditions using RGB data. Further, the ENVI LiDAR algorithm seems better suited for full canopies as all but the RGB data sets exhibit increases in estimated trees in these conditions. Perhaps these point clouds display stronger agreement as far as 'dispersal characteristics' used to delineate trees (Exelis Visual Information Solutions 2010). Phenological differences observed in leaf-on conditions provide estimates that more closely resemble *in situ* measurements in terms of height for RGB point clouds, but in both seasons discrete band spectral point clouds (red and green in November; red edge in July) outperform the RGB despite coarser spatial resolution. Radial estimates using this method seem a bit noisy, but the seasonal consideration is similar in that under-predictions of radial dimensions are fewer with leaf-on canopies, providing better surfaces to resolve using the SfM-MVS approach. It is possible that other methods involving various filtering techniques would be more appropriate for extraction of this component of vegetation structure (Chen et al. 2006; Lindberg and Holmgren 2017).

Radial estimates are markedly different between data collected in senesced (November) and full canopy conditions (July). In general, crown radii were better predicted under full canopy conditions than with data collected in senesced conditions. In July, the red edge data provided marginally weaker estimates than the RGB point cloud for all metrics despite coarser spatial resolution. However, these data better capture the quantity of *in situ* individuals sampled within the study site, and larger sample sizes are likely to increase disagreement and error metrics.

Due to the varying tree vector sample sizes, MAE, while descriptive, can be misleading in this context. Interestingly, the RGB sample was reduced from the November flight to the July flight estimates, while all other sample sizes increased. It is reasonable to expect larger samples to exhibit higher MAE as there are more opportunities to increase this statistic as sample sizes increase. A crown estimate that may have been ignored entirely in another dataset holds potential to skew this statistic, but still has potential to provide an analyst valuable information regarding land function despite erroneous height or radial measurement where stem count or recruitment frequency is of interest (Shulz et al. 2018). Despite three times finer spatial resolution than the multispectral datasets, the RGB data explain only slightly more of the variation in UAS estimates than the red edge data in full canopy conditions. What is more, datasets with greater spectral detail data more fully represent the *in situ* crowns measured during this season, as well as align better with randomly classified points. These results hold potential to improve upon studies that seek to quantify above ground biomass or post-fire recovery, for example, as much of the recent work relies upon the use of an RGB CHM (Alonzo et al. 2018; Laringa and Brotons 2019).

The manner in which the watershed segmentation is implemented in the ENVI LiDAR software likely introduced error in radial comparisons, as crown dimensions rarely exhibit circular conditions in this study area yet are assumed to be symmetric by the software. Field data includes independent measurements in all four cardinal directions while ENVI LiDAR crown estimates are produced based upon the extent of the crown as estimated by a boundary based segmentation of a two-dimensional digital surface model. The radial estimates could possibly be improved by using methods that more closely resemble true crown dimensions in multiple axes tools (Dalponte and Coomes 2016). Further, since Delaunay triangulation was used to create the DSM within Pix4D, underestimated crowns may be prevalent, particularly in autumnal conditions and results may vary using methods that provide a smoothed output such as inverse distance weighting.

We expect some location error with respect to validation points despite differential correction as well as with point clouds as a result of forgoing the use of labor-intensive ground control. Thus, we consider quantity error to be the most descriptive metric used, as allocation error is expected. Results of this exercise reveal that the denser RGB point cloud outperforms the datasets with refined spectral information during the senesced period ($Q_{RGB} = 0.14$), but the opposite is true in full canopy conditions with all other datasets showing lower quantity disagreement ($Q_{RGB} = 0.21$, $Q_{green} = 0.10$, $Q_{red} = 0.15$, $Q_{red\ edge} = 0.14$, $Q_{NIR} = 0.18$). This exercise suggests that the presence of active chlorophyll and continuous canopy surfaces aid in estimating fractional woody coverage in largely vegetated sites.

Results of the tests of quantity and allocation disagreement highlight the importance and value of the use of rigorous ground control and highly accurate GNSS for analysis of hyperspatial resolution datasets if trying to validate in the field. The study site was chosen due to its heterogeneous nature, but the accuracy of the handheld Trimble GeoXT 6000 even after differential correction, was far too coarse to confidently relate to point cloud estimates with centimetric resolution, as even a meter or two in any direction can be cause for false classification. Furthermore, under-predictions in radial dimensions and the circular output of the estimated crowns leave gaps between trees that could likely be accounted for using more robust delineation tools (Dalponte and Coomes 2016). But regarding the goal of sampling a study area using UAS point clouds to estimate metrics of vegetation structure, all point clouds seem reasonable in terms of providing an objective description of vegetation in a region of interest. Despite these considerations, this study displays the utility of leveraging NIR data via a lightweight multispectral sensor for estimating height and radial dimensions of vegetation.

4. Conclusions

The results demonstrate that detailed spectral information in discrete bands both within and beyond the visible portion of the spectrum can improve the ability to estimate structural characteristics of woody vegetation, despite SfM-MVS point clouds being substantially less dense than RGB data. We conclude that more detailed spectral information within and beyond the visible spectrum provides more nuance than typically collected with a standard RGB sensor. Furthermore, information beyond visible light, such as the red edge band, provides additional information valuable to discrimination between individuals even at relatively coarse resolution. These results can be considered an initial effort towards determination of appropriate data for studies of vegetation structure using SfM-MVS and imply that spectral information in the red to NIR portion of the spectrum is valuable for estimating height metrics of vegetation structure while employing a structure from motion approach. The methods used here are possibly applicable precision agriculture (Chu et al. 2018), forestry (Alonzo et al. 2018), or any other UAS study where vegetation height is of interest and the time-cost of a thorough field survey too great. Consistent with results of studies that include multispectral information with LiDAR data to improve tree crown delineation (Lindberg and Holmgren 2017), multispectral information should be considered for SfM-MVS applications. What is more, off the shelf products used for UAS sampling can objectively and quickly provide valuable information about vegetation structure that could potentially be upscaled to imagery with greater spatial and temporal resolution.

Acknowledgments

This research is supported by a United States National Science Foundation (NSF) grant (#1560700). We are grateful for the careful comments and critiques of the anonymous reviewers that helped us to improve this manuscript.

Declaration of interest statement

No potential conflict of interest was reported by the authors.

References

Adelabu, S., O. Mutanga and E. Adam. 2014. Evaluating the impact of red-edge band from Rapideye image for classifying insect defoliation levels. *ISPRS Journal of Photogrammetry and Remote Sensing* 95, 34-41 doi: 10.1016/j.isprsjprs.2014.05.013

Alonzo, M., H. E. Andersen, D. Morton and B. Cook. 2018. Quantifying Boreal Forest Structure and Composition Using UAV Structure from Motion. *Forests* 9(3): 119. doi:10.3390/f9030119

Avery, T.E., Burkhartn, H.E. 2001. Forest Measurements, 5th edn. McGraw-Hill, Boston.

Chen, Q., D. Baldocchi, P. Gong, and M. Kelly. 2006. Isolating Individual Trees in a Savanna Woodland Using Small Footprint Lidar Data. *Photogrammetric Engineering and Remote Sensing* 72(8): 923-932. doi:0099-1112/06/7208–0923

Chu, T., M. J. Stark, M. J. Brewer, S. C. Murray, and L. S. Pruter. 2018. Characterizing canopy height with UAS structure-from-motion photogrammetry-results analysis of a maize field trial with respect to multiple factors. *Remote Sensing Letters* 9(8): 753-762. doi: 10.1080/2150704X.2018.1475771

Cunliffe, A. M., R. E. Brazier and K. Anderson. 2016. Ultra-fine grain landscape-scale quantification of dryland vegetation structure with drone-acquired structure-from-motion photogrammetry. *Remote Sensing of Environment* 183: 129-143.doi:https://10.1016/j.rse.2016.05.019

Curran, P. 1980. Multispectral remote sensing of vegetation amount. Progress in Physical Geography: *Earth and Environment* 4(3): 315 – 341.

Dalponte, M. and D. A. Coomes. 2016. Tree-centric mapping of forest carbon density from airborne laser scanning and hyperspectral data. *Methods in Ecology and Evolution* 7: 1236-1245. doi: 10.1111/2041-210X.12575

Dandois, J. P. and E. C. Ellis. 2010. Remote Sensing of Vegetation Structure Using Computer Vision. *Remote Sensing* 2: 1157-1176. doi:=10.3390/rs2041157

DJI. 2018. DJI Mavic Pro wherever you go. Available at https://www.dji.com/mavic (last accessed March 2018).

Exelis Visual Information Solutions. 2010. Name of the manual. Boulder, Colorado: Exelis Visual Information Solutions. Available online: https://www.harrisgeospatial.com/docs/

Filella I. and J. Penuelas. 1994. The red edge position and shape as indicators of plant chlorophyll content, biomass, and hydric status. *International Journal of Remote Sensing* 15(7): 1459-1470.

Jakubowski, M., W. Li, Q. Guo and M. Kelly. 2013. Delineating Individual Trees from Lidar Data: A Comparison of Vector- and Raster-based Segmentation Approaches. *Remote Sensing* 5: 4163-4186. doi:10.3390/rs5094163

Larrinaga, A. & L. Brotons. 2019. Greenness Indices from a Low-Cost UAV Imagery as Tools for Monitoring Post-Fire Forest Recovery. *Drones* 3(1): 6. doi:10.3390/drones3010006

Lindberg, E. and J. Holmgren. 2017. Individual Tree Crown Methods for 3D Data from Remote Sensing. *Current Forestry Reports* 3: 19-31. doi:10.1007/s40725-017-0051-6

Mayr, M. J., S. Malß, E. Ofner and C. Samimi. 2017. Disturbance feedbacks on the height of woody vegetation in a savannah: a multi-plot assessment using an unmanned aerial vehicle (UAV). *International Journal of Remote Sensing* 1-25. doi:10.1080/01431161.2017.1362132.

Padró, J.-C., F.-J. Muñoz, J. Planas and X. Pons. 2019. Comparison of four UAV georeferencing methods for environmental monitoring purposes focusing on the combined use with airborne and satellite remote sensing platforms. *International Journal of Applied Earth Observation and Geoinformation* 75: 130-140. doi:10.1016/j.jag.2018.10.018

Pontius, R. G. and M. Millones. 2011. Death to Kappa: birth of quantity disagreement and allocation disagreement for accuracy assessment. *International Journal of Remote Sensing* 32: 4407-4429. doi: 10.1080/01431161.2011.552923

Pix4Dmapper 3.3 USER MANUAL. Pix4D SA: Lausanne, Switzerland, 2017.

Salamí, E., C. Barrado and E. Pastor. 2014. UAV Flight Experiments Applied to the Remote Sensing of Vegetated Areas. *Remote Sensing* 6: 11051-11081. doi:10.3390/rs61111051.

Schulz, K., M. Guschal, I. Kowarik, J. S. Almeida-Cortez, E. V. S. B. Sampaio. 2018. Grazing, forest density, and carbon storage: towards a more sustainable land us in Caatinga dry forests of Brazil. *Regional Environmental Change* 18: 1969-1981. doi:10.1007/s1011

Smith, M.W., J. L Carrivick, and D. J. Quincey. 2015. Structure from motion photogrammetry in physical geography. Progress in Physical Geography 40 (2): 247 - 275. doi:10.1177/0309133315615805.

Tucker, C. J. 1979. Red and photographic infrared linear combinations for monitoring vegetation. *Remote Sensing of the Environment* 8:127-150. doi:10.1016/0034-4257(79)90013-0.

Turner, D., A. Lucieer and L. Wallace. 2014. Direct Georeferencing of Ultrahigh-Resolution UAV Imagery. *IEEE Transactions on Geoscience and Remote Sensing* 52: 2738-2745. doi: 10.1109/TGRS.2013.2265295.

Zahawi, R. A., J. P. Dandois, K. D. Holl, D. Nadwodny, J. L. Reid and E. C. Ellis. 2015. Using lightweight unmanned aerial vehicles to monitor tropical forest recovery. *Biological Conservation* 186: 287-295. doi:10.1016/j.biocon.2015.03.031

Figure 1

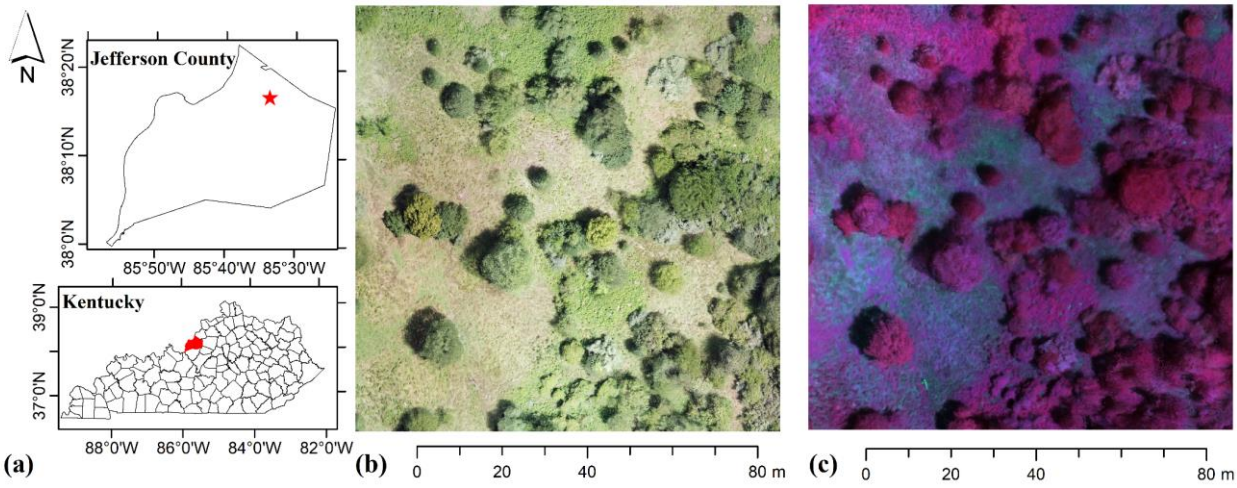

Figure 2

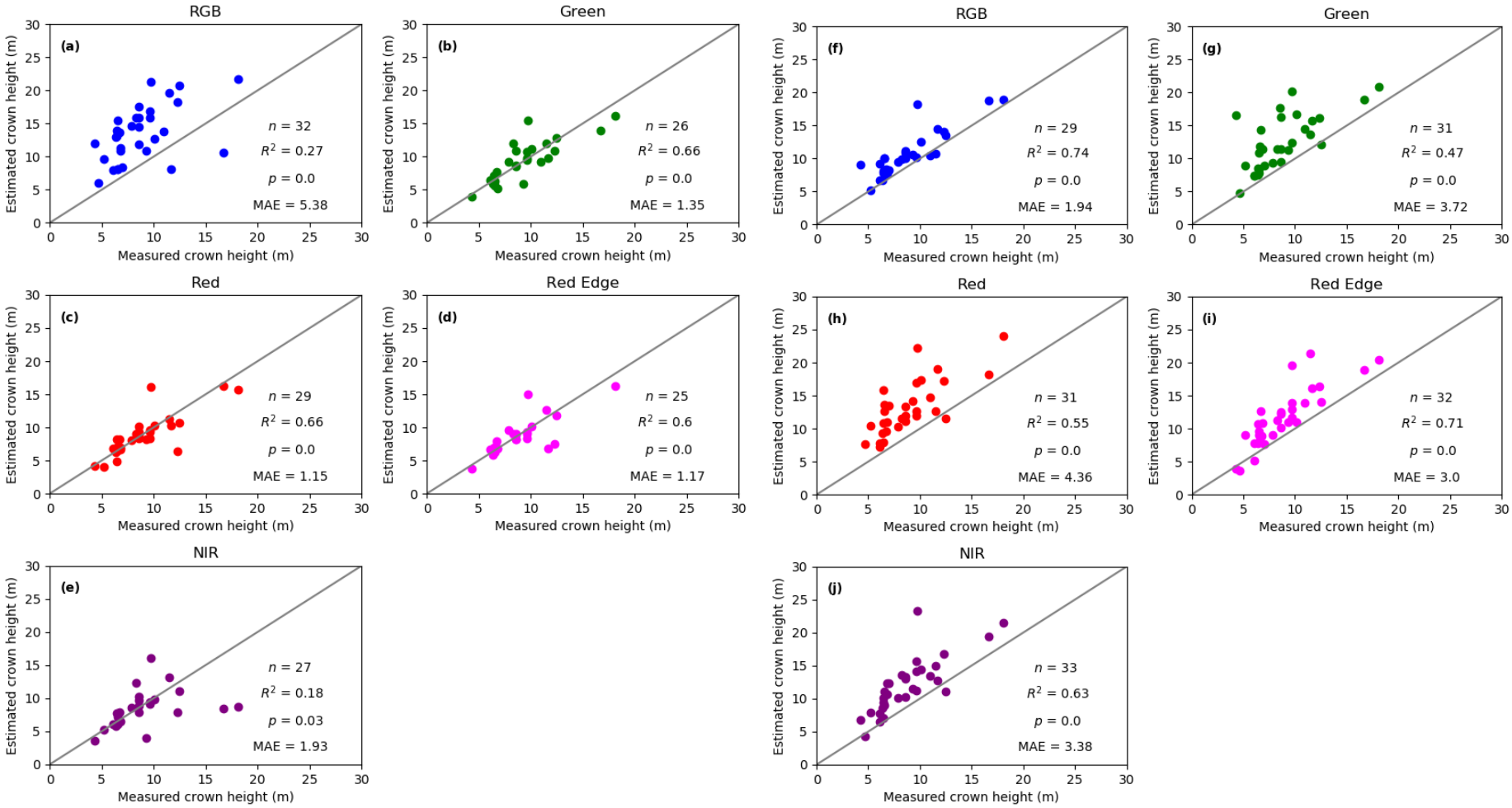
RGB
(a)
n = 32
R^2 = 0.27
p = 0.0
MAE = 5.38
Green
(b)
n = 26
R^2 = 0.66
p = 0.0
MAE = 1.35
RGB
(f)
n = 29
R^2 = 0.74
p = 0.0
MAE = 1.94
Green
(g)
n = 31
R^2 = 0.47
p = 0.0
MAE = 3.72
Red
(c)
n = 29
R^2 = 0.66
p = 0.0
MAE = 1.15
Red Edge
(d)
n = 25
R^2 = 0.6
p = 0.0
MAE = 1.17
Red
(h)
n = 31
R^2 = 0.55
p = 0.0
MAE = 4.36
Red Edge
(i)
n = 32
R^2 = 0.71
p = 0.0
MAE = 3.0
NIR
(e)
n = 27
R^2 = 0.18
p = 0.03
MAE = 1.93
NIR
(j)
n = 33
R^2 = 0.63
p = 0.0
MAE = 3.38
Estimated crown height (m)
Measured crown height (m)

Figure 3

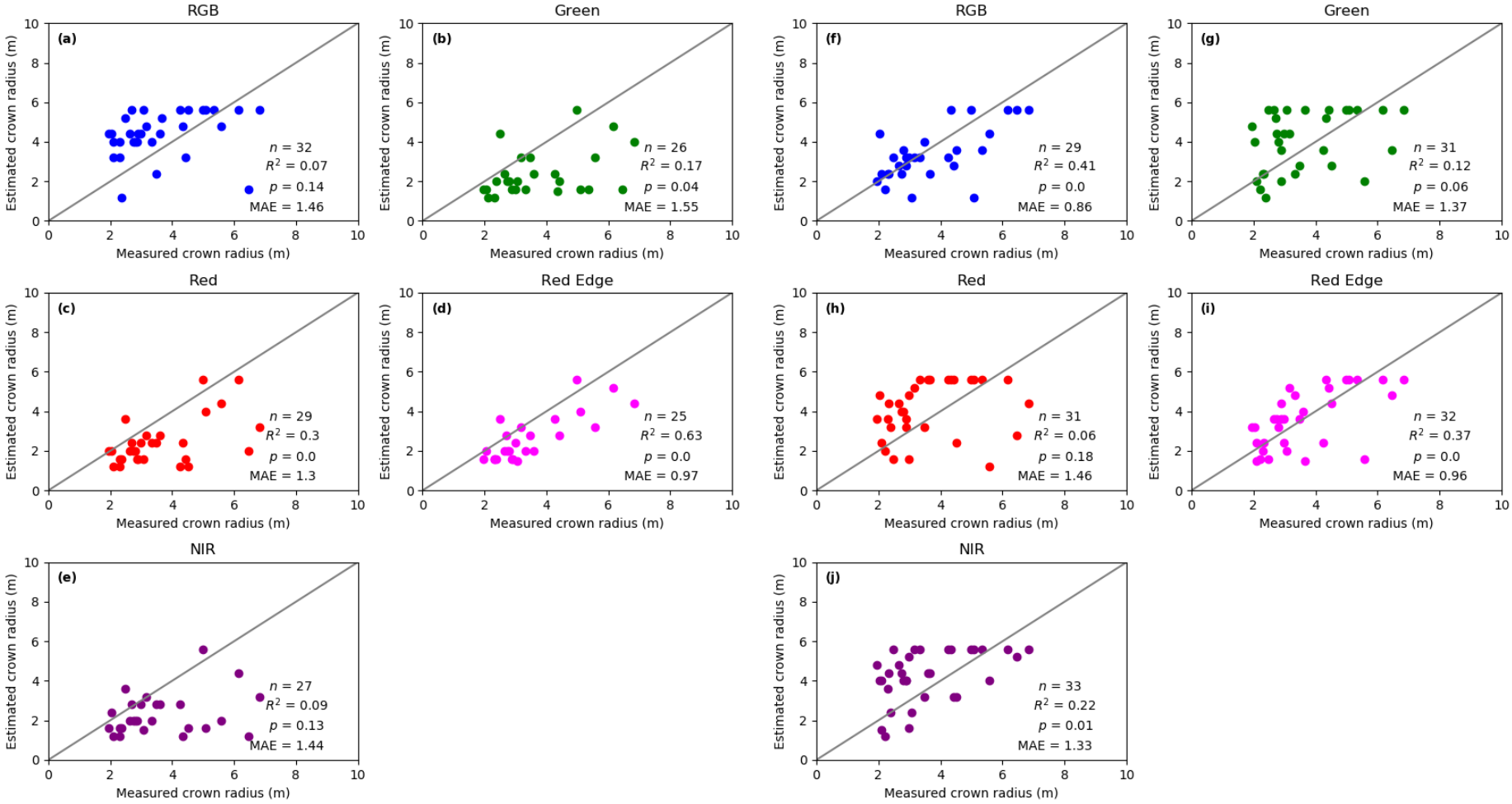
RGB
(a)
n = 32
R² = 0.07
p = 0.14
MAE = 1.46
Green
(b)
n = 26
R² = 0.17
p = 0.04
MAE = 1.55
RGB
(f)
n = 29
R² = 0.41
p = 0.0
MAE = 0.86
Green
(g)
n = 31
R² = 0.12
p = 0.06
MAE = 1.37
Red
(c)
n = 29
R² = 0.3
p = 0.0
MAE = 1.3
Red Edge
(d)
n = 25
R² = 0.63
p = 0.0
MAE = 0.97
Red
(h)
n = 31
R² = 0.06
p = 0.18
MAE = 1.46
Red Edge
(i)
n = 32
R² = 0.37
p = 0.0
MAE = 0.96
NIR
(e)
n = 27
R² = 0.09
p = 0.13
MAE = 1.44
NIR
(j)
n = 33
R² = 0.22
p = 0.01
MAE = 1.33
Estimated crown radius (m)
Measured crown radius (m)

Figure 1. Panel *a* – Location maps for study region (marked by the red star) in Jefferson, County, Kentucky (highlighted in red) known locally as E.P "Tom" Sawyer State Park. A portion of the park exhibiting heterogeneity in terms of structure and species was chosen with the aim of successful delineation between individuals and vegetation types. Panel *b* displays a portion of the RGB orthomosaic (~3.7cm ground sampling distance (GSD)) and panel *c* a false color composite (NIR, red, green) using the Parrot Sequoia data (~10.4 cm GSD).

Figure 2. Height estimate comparison scatterplots (*a-e*: November; *f-j* : July);
Plots *a* and *f* display correlation between *in situ* height measurements and UAS CHM estimates for the baseline RGB sensor. Plots *b-e* and *g-j* display correlation between field measurements and UAS CHM estimates for red, green, red edge, and NIR bands of data respectively. All plots include a 1:1 line for visual aid.

Figure 3. Radial estimate comparison scatterplots (*a-e*: November; *f-j* : July);
Plots *a* and *f* display correlation between *in situ* crown measurements and UAS CHM estimates for the baseline RGB sensor. Plots *b-e* and *g-j* display correlation between field measurements and UAS CHM estimates for red, green, red edge, and NIR bands of data respectively. All plots include a 1:1 line for visual aid.

Code available @ https://github.com/neko1010/Tom_Sawyer